



**HAL**  
open science

## **Disrupted function of lactate transporter MCT1 , but not MCT4 , in Schwann cells affects the maintenance of motor end-plate innervation**

Filipa Bouçanova, Gill Pollmeier, Katalin Sandor, Carlos Morado Urbina, Jik Nijssen, Jean-jacques Médard, Luca Bartesaghi, Luc Pellerin, Camilla I Svensson, Eva Hedlund, et al.

### ► To cite this version:

Filipa Bouçanova, Gill Pollmeier, Katalin Sandor, Carlos Morado Urbina, Jik Nijssen, et al.. Disrupted function of lactate transporter MCT1 , but not MCT4 , in Schwann cells affects the maintenance of motor end-plate innervation. *Glia*, 2021, 69 (1), pp.124-136. 10.1002/glia.23889 . hal-03366045

**HAL Id: hal-03366045**

**<https://cnrs.hal.science/hal-03366045>**

Submitted on 5 Oct 2021

**HAL** is a multi-disciplinary open access archive for the deposit and dissemination of scientific research documents, whether they are published or not. The documents may come from teaching and research institutions in France or abroad, or from public or private research centers.


L'archive ouverte pluridisciplinaire **HAL**, est destinée au dépôt et à la diffusion de documents scientifiques de niveau recherche, publiés ou non, émanant des établissements d'enseignement et de recherche français ou étrangers, des laboratoires publics ou privés.



Distributed under a Creative Commons Attribution 4.0 International License

## RESEARCH ARTICLE

# Disrupted function of lactate transporter MCT1, but not MCT4, in Schwann cells affects the maintenance of motor end-plate innervation

Filipa Boučanová<sup>1,2</sup> | Gill Pollmeier<sup>1</sup> | Katalin Sandor<sup>3</sup> | Carlos Morado Urbina<sup>3</sup> | Jik Nijssen<sup>1</sup> | Jean-Jacques Médard<sup>1,2</sup> | Luca Bartesaghi<sup>1,2</sup> | Luc Pellerin<sup>4,5,6</sup> | Camilla I Svensson<sup>3</sup> | Eva Hedlund<sup>1</sup> | Roman Chrast<sup>1,2</sup> 

<sup>1</sup>Department of Neuroscience, Karolinska Institutet, Stockholm, Sweden

<sup>2</sup>Department of Clinical Neuroscience, Karolinska Institutet, Stockholm, Sweden

<sup>3</sup>Department of Physiology and Pharmacology and Center for Molecular Medicine, Karolinska Institutet, Stockholm, Sweden

<sup>4</sup>Department of Physiology, University of Lausanne, Lausanne, Switzerland

<sup>5</sup>Centre de Résonance Magnétique des Systèmes Biologiques, UMR5536 CNRS, LabEx TRAIL-IBIO, Université de Bordeaux, Bordeaux Cedex, France

<sup>6</sup>Inserm U1082, Université de Poitiers, Poitiers Cedex, France

## Correspondence

Roman Chrast, Department of Neuroscience, Karolinska Institutet, Stockholm, Sweden.  
Email: roman.chrast@ki.se

## Funding information

Agence Nationale de la Recherche, Grant/Award Number: ANR-10-IDEX-03-02; Knut och Alice Wallenbergs Stiftelse; Vetenskapsrådet, Grant/Award Numbers: 2013-8373, 2015-02394, 2016-02112; University of Lausanne; Swedish StratNeuro

## Abstract

Recent studies in neuron-glia metabolic coupling have shown that, in the CNS, astrocytes and oligodendrocytes support neurons with energy-rich lactate/pyruvate via monocarboxylate transporters (MCTs). The presence of such transporters in the PNS, in both Schwann cells and neurons, has prompted us to question if a similar interaction may be present. Here we describe the generation and characterization of conditional knockout mouse models where MCT1 or MCT4 is specifically deleted in Schwann cells (named MCT1 and MCT4 cKO). We show that MCT1 cKO and MCT4 cKO mice develop normally and that myelin in the PNS is preserved. However, MCT1 expressed by Schwann cells is necessary for long-term maintenance of motor end-plate integrity as revealed by disrupted neuromuscular innervation in mutant mice, while MCT4 appears largely dispensable for the support of motor neurons. Concomitant to detected structural alterations, lumbar motor neurons from MCT1 cKO mice show transcriptional changes affecting cytoskeletal components, transcriptional regulators, and mitochondria related transcripts, among others. Together, our data indicate that MCT1 plays a role in Schwann cell-mediated maintenance of motor end-plate innervation thus providing further insight into the emerging picture of the biology of the axon-glia metabolic crosstalk.

## KEYWORDS

monocarboxylate transporter, motor neuron, PNS, RNA-Seq, Schwann cell

## 1 | INTRODUCTION

The peripheral nervous system (PNS) is formed by sensory and motor neurons whose cellular bodies are located in dorsal root ganglia and spinal cord gray matter, respectively. Both types of neurons extend long axonal projections into peripheral tissues such as skin, glands,

and muscles where they exert their functions of detecting sensory stimuli and executing motor responses such as muscle contraction. These long peripheral axons are bundled into nerves that contain Schwann cells (SCs), the myelinating glia of the PNS, and are enveloped by connective tissue generated by fibroblasts. The long distances between the neuronal cell body and the distal regions of the

This is an open access article under the terms of the Creative Commons Attribution License, which permits use, distribution and reproduction in any medium, provided the original work is properly cited.

© 2020 The Authors. *Glia* published by Wiley Periodicals LLC

axon, and the fact that axons are isolated from the extracellular environment by surrounding myelinating and non-myelinating SC, raise the question of how neurons obtain energy-rich substrates to sustain their metabolism (Hirrlinger & Nave, 2014; Nave, 2010). It stands to reason that transport of such nutrients from the soma to the periphery would be slow and inefficient (for comparison, transport of glycolytic enzymes occurs at a speed of 0.02  $\mu\text{m/s}$ ; Brady & Lasek, 1981), and that direct uptake from the extracellular space at the exposed nodes of Ranvier (less than 1% of the total membrane surface area) might be insufficient to meet the energetic needs of active neurons (Nave, 2010). One possibility is that SC are not simply insulators and passive spectators of neuronal function, but instead they act as metabolic intermediaries, taking up glucose from the blood or interstitial space, converting it to small energetic metabolites such as lactate and pyruvate and finally shuttling these substrates to the underlying neuron, where they can be used for mitochondrial oxidative phosphorylation and energy production.

In the CNS, oligodendrocytes and astrocytes express monocarboxylate transporters (MCT) 1 and 4 (1 is expressed in both cell types, 4 in astrocytes exclusively). These glial cells appear to be metabolically coupled to neurons in some CNS regions such as the spinal cord, brain cortex, and hippocampus, providing them with lactate that can be taken up by high-affinity neuronal MCT2 (Lee et al., 2012; Machler et al., 2016; Pierre, Magistretti, & Pellerin, 2002; Suzuki et al., 2011). Other regions, like the corpus callosum, seem to rely primarily on glia-derived glucose (Meyer et al., 2018). MCTs are proton-coupled transporters of monocarboxylates (lactate, pyruvate, and ketone bodies) (Halestrap, 2013). They present different affinities to their substrates (MCT2 has the highest affinity, followed by MCT1 and MCT4 having the lowest affinity) and are expressed in different cell types, which may be related to the cells status as net producers or consumers of monocarboxylates (Halestrap, 2013). In the PNS, SC express MCT1, 2 and 4 whereas DRG neurons express MCT1 and 2 (Domenech-Estevéz et al., 2015; Morrison et al., 2015). The presence of different MCTs on both partners in the PNS suggests a metabolic coupling similar to the one operating in the CNS.

In order to evaluate the possible role of MCTs in the crosstalk between glia and underlying axons we generated and characterized two conditional knockout models in which MCT1 or MCT4 were eliminated specifically in SC using MPZ-Cre-driven recombination of floxed MCT alleles. We find that MCT1 (but not MCT4) expression in SC is necessary for maintenance of neuromuscular junction innervation. This is associated with transcriptional changes in lumbar motor neurons of MCT1 conditional knockout mice, suggesting that SC's metabolic support to axons is necessary for proper maintenance of motor neurons.

## 2 | MATERIALS AND METHODS

### 2.1 | Animals

Mice carrying floxed alleles of *Slc16a1/MCT1* (exon 5, *MCT1<sup>fE5</sup>*) or *Slc16a3/MCT4* (exons 3–5, *MCT4<sup>fE3–5</sup>*) were developed in

collaboration with Prof. Luc Pellerin by Cyagen, Santa Clara CA, and back-crossed to a C57BL/6 genetic background for at least 10 generations to generate lines C57/Bl/6.MCT1tm1flox and C57/Bl/6.MCT4tm1flox. Each of these lines was then crossed with B6N.FVB-Tg(Mpz-cre)26Mes/J (Jackson Laboratories; Feltri et al., 1999) for SC-specific deletion of MCT1 or MCT4. Homozygous floxed animals carrying one copy of the MPZ-Cre allele were used as cKO and the Cre-negative littermates were used as control (henceforth referred to as MCT1 control and MCT1 cKO or MCT4 control and MCT4 cKO).

Animals were kept in specific-pathogen-free (SPF) conditions, under a 12 hr light–dark cycle, with food and water ad libitum. All experiments were performed at Karolinska Institutet's Department of Comparative Medicine animal facility with approval by the Stockholm Ethics Committee (Stockholms djurförsöksetiska nämnd, ethical permits N79/15 and 7448-2018 awarded to Roman Chrast and Camilla Svensson, respectively) and conformed to European Directive 2010/63/EU as well as local guidelines.

### 2.2 | PCR and qPCR

Animals were genotyped by PCR at 21 days of age using genomic DNA obtained from ear biopsies. Primer sequences used and expected molecular weights are shown in Supplemental Table 1.

For confirmation of Cre-mediated recombination, sciatic nerves were collected at 1 month of age, stripped of peri-epineurium, flash frozen in liquid nitrogen, and stored at  $-80^{\circ}\text{C}$  until further processing. Tissues were homogenized in QIAzol using a Tissue Lyser II apparatus and stainless-steel beads and mRNA was extracted using QIAGEN RNeasy Lipid Tissue Mini Kit according to the manufacturer's instructions. An equal amount of RNA for each sample was retrotranscribed using Takara PrimeScript RT-PCR Kit and qPCR was performed on 7500 Fast Real-Time PCR System instrument (Applied Biosystems) using SybrGreen master mix (Roche). Primer sequences can be found in Supplemental Table 1. Relative mRNA expression was determined using the  $-\Delta\Delta\text{Ct}$  method and results are expressed as average fold change to control mean  $\pm$  SD. Statistical analysis was done with GraphPad Prism 8 on  $\Delta\text{Ct}$  values (gene Ct-reference gene Ct) using unpaired two-tailed *t*-test with Welch's correction. *p*-values are indicated in figures and statistical significance was recognized when  $p < .05$ .

### 2.3 | Western blotting and immunohistochemistry of teased fibers

To further validate MCT1 and MCT4 inactivation, sciatic nerve endoneuria were lysed using a Tissue Lyser II apparatus and stainless-steel beads to obtain protein extracts (lysis buffer containing 5% SDS, 5 mM EDTA and 80 mM Tris-HCl, supplemented with 1X cComplete™ Mini EDTA-free Protease Inhibitor Cocktail (Roche), 1 mM NaF and 1 mM  $\text{NaVO}_4$ ). Between 20 and 50  $\mu\text{g}$  of proteins (quantified using the Pierce BCA Protein Assay Kit, Thermo Scientific) were separated by SDS-PAGE on 12.5% polyacrylamide gels and transferred onto



Immobilon-FL (Millipore) or nitrocellulose (Thermo Scientific) membranes. Membranes were blocked in 5% milk in tris-buffered saline (TBS) with 0.05% Tween-20 for 1 hr at room temperature, washed and incubated with primary antibody (rabbit anti-MCT1 [Stumpf et al., 2019] or rabbit anti-MCT4 [Santa Cruz]) for 48 or 24 hr, respectively, at 4°C with agitation. After washing, membranes were incubated with secondary antibodies for 2 hr at room temperature, scanned using the Odyssey Infrared Imaging System and analyzed with Image Studio Software (Li-Cor, Inc.). Membranes were re-blocked, stained for tubulin and imaged the next day. For teased fiber preparation from MCT4 cKO mice, sciatic nerves were freshly dissected and fixed in 4% paraformaldehyde for 15 min at room temperature. After washing in PBS, nerves were cut into smaller pieces, stripped of peri-epineurium and teased on TESPA-coated slides using fine insect pins. Teased fibers were allowed to dry and kept at -80°C until the next day. For immunohistochemistry, fibers were permeabilized with Triton X100 0.1% for 15 min at room temperature, blocked in a solution of 5% BSA, 1% NGS, and Triton X100 0.1% for 1 hr and incubated with rabbit anti-MCT4 primary antibody (Santa Cruz) overnight at room temperature. After washing, fibers were incubated with a secondary antibody, counterstained with DAPI and mounted with Vectashield mounting medium. Antibody references and dilutions can be found in Supplemental Table 2.

## 2.4 | Electron microscopy and analysis of sciatic nerve structure

One-year old mice were anesthetized with isoflurane and sacrificed by decapitation. Sciatic nerves and spinal roots were dissected and immediately fixed in 2.5% glutaraldehyde in 0.1 M sodium cacodylate buffer for 2 hr at room temperature, followed by overnight washing in the same buffer. Samples were stained for 4 hr in 1% OsO<sub>4</sub> in cacodylate buffer followed by dehydration in increasing concentrations of ethanol. Then, tissues were infiltrated with propylene oxide and embedded in Epoxy Embedding Medium (Sigma) (modified from Bartesaghi et al., 2015).

For *g*-ratio quantification, samples were sectioned at 0.5 μm thickness using an Ultracut E (Reichert-Jung) ultramicrotome and stained with toluidine blue in 0.1 M sodium borate buffer. Images were acquired using Zeiss Axioskop 40 light microscope at ×100 magnification and *g*-ratio determined using Fiji software (Schindelin et al., 2012) and *g*-ratio calculator plugin as previously described (Arnaud et al., 2009). An average of 859 fibers of one sciatic nerve section per sample were quantified, three samples per genotype were used.

For analysis of Remak bundles, samples were sectioned at 50–60 nm thickness using a Leica EM UC7 ultramicrotome (Leica, Wien, Austria), transferred onto formvar stabilized slot grids and contrasted with uranyl acetate followed by lead citrate. Sections were examined in a Tecnai Spirit BioTWIN transmission electron microscope (FEI Company, Eindhoven, The Netherlands) operated at 100 kV. Digital images were acquired using a 2kx2k Veleta CCD camera (Olympus Soft Imaging Solutions, GmbH, Münster, Germany).

Images of ×1,200 magnification were used to determine the area occupied by Remak bundles (one section per sample was quantified, three samples per genotype). Images of ×11,000 magnification were used to determine number of small unmyelinated fibers per bundle and the diameter of the largest unmyelinated fibers observed. Thirty to fifty randomly selected bundles of one section per sample were quantified, three samples per genotype were used. The experimenter was blinded to the samples' genotype during image analysis. Statistical analysis was performed using an unpaired two-tailed *t*-test with Welch's correction.

## 2.5 | Motor and sensory nerve conduction studies

Nerve conduction velocity studies were performed using a Nicolet Viking electromyograph system. One-year old animals were anesthetized intraperitoneally with a mixture of ketamine and xylazine. Animals were positioned face down on a styrofoam surface and platinum needle electrodes were inserted in the interdigital muscles to record motor nerve conduction velocity. Stimulating electrodes were placed near the Achilles tendon and sciatic notch and a supramaximal stimulation was applied at 0.5 Hz and 0.1 ms duration. Velocity was calculated by dividing the difference in response latency for each stimulation by the distance between the stimulation sites. Two to three separate measurements were recorded on each leg and the results are expressed as mean velocity per animal. Sensory nerve conduction velocity was recorded subdermally at the base of the tail with stimulation distally at 3 cm, with supramaximal stimulation of 0.7 Hz frequency and 0.1 ms duration. Results are mean of 10 sweeps for a single measurement per animal. All measurements were performed at room temperature. After measurements, animals were sacrificed for tissue collection.

## 2.6 | Motor and sensory behavioral tests

Motor behavior was assessed using the CatWalk system (Noldus Information Technology, The Netherlands) as previously described (Angeby Moller et al., 2018). Briefly, 1-year old mice of both sexes were habituated to the room for 30 min and then allowed to cross the Catwalk system three times. The mouse's home cage was used as bait at the opposite end of the CatWalk. After two training sessions on separate days, baseline measurements were recorded using the Catwalk XT software version 10.6. The parameters analyzed are mentioned in the results section. Mechanical hypersensitivity was assessed using the Marstock OptiHair filaments (Marstock, Germany) and the up-down testing method was used (Chaplan, Bach, Pogrel, Chung, & Yaksh, 1994; Dixon, 1980). Briefly, mice were habituated to a testing enclosure with wire mesh bottom for about an hour prior to testing. Withdrawal thresholds were assessed by a set of filaments with increasing forces, applied perpendicularly to the center of the plantar surface of the hind paw for a maximum of 5 s, or until a brisk response was observed. Results are expressed as 50% threshold

values in grams (g), presented as average of the values taken from both hind legs. Mice were habituated to the testing environment on at least two separate occasions. Cold sensitivity was assessed using the acetone drop test. Mice were habituated to the same enclosure with a wire mesh bottom, where one acetone drop was applied gently to the plantar side of one hind paw with the aid of a 1 ml syringe. The time spent with nocifensive reaction (licking, shaking, biting the hind leg) was recorded for 60 s. The test was repeated three times on each leg with 30 min test-free period between sessions. Data are presented as time spent reacting to acetone in seconds (s). Mice were habituated to the testing environment on at least two separate occasions. Heat sensitivity was assessed using a modified Hargreaves box (Dirig, Salami, Rathbun, Ozaki, & Yaksh, 1997). Mice were placed on the glass surface in Plexiglas containers and allowed to habituate to the test environment prior to testing. Paw withdrawal, observed as a brisk reaction, was evoked by an increasing light stimulus positioned to the middle of the footpad. To prevent thermal exposure damage, the stimulus is turned off at a cut-off time of 20 s or 55°C. Data are presented as paw withdrawal latency in seconds. After assessing the withdrawal latency for one paw of all mice, the second paw was measured and this was repeated three times, with 30 min test-free period in-between sessions. Average of both legs was calculated. Mice were habituated to the testing environment on at least two separate occasions. The experimenter was blinded to the animals' genotypes for the duration of the tests.

## 2.7 | Immunohistochemistry and analysis of distal innervation

One-year old animals were sacrificed and dissected to collect gastrocnemius muscle and hind paw skin for cryosectioning and immunohistochemistry. Muscles of 6-month old animals were also obtained for confirmation analysis of muscular innervation. Briefly, gastrocnemius muscle was fixed in 4% PFA in PBS for 20 min, washed in PBS and cryopreserved in 30% sucrose in PBS overnight, prior to embedding in optimal cutting medium (OCT). Similarly, skin from the hind paws (containing the walking pads) was dissected, fixed in Zamboni's fixative for 2 hr, washed and cryopreserved before embedding in OCT. Samples were stored at -80°C until further processing. Tissues were sectioned in a Cryostat NX70 cryostat at -20°C and collected on Superfrost Plus glass slides (25 µm longitudinal sections for muscle, 50 µm cross-sections for skin). Muscle sections were permeabilized and blocked in a solution of 5% BSA, 1% NGS and triton 0.1% for 4 hr, followed by overnight incubation with primary antibodies at 4°C. Following washing, samples were incubated with the secondary antibody and fluorescently labeled bungarotoxin for 2 hr at room temperature, counterstained with DAPI and mounted with Vectashield mounting medium. Skin sections were incubated on a slide in blocking solution (1% NGS, 0.15% Triton X-100 in PBS) for 4 hr at room temperature, followed by overnight incubation with the primary antibody at 4°C and the secondary antibody 2 hr at room temperature. Sections were counterstained with DAPI and mounted with Vectashield. Primary and

secondary antibodies and stains can be found in Supplemental Table 2.

To characterize the innervation status of neuromuscular junctions (NMJ), ×20 magnification images were acquired using a Zeiss Observer Z1 epifluorescence microscope and an ORCA-Flash4.0 LT camera (Hamamatsu Photonics, Japan). One hundred randomly selected NMJs per sample were classified as fully innervated (>30% overlap between bungarotoxin staining and SV2/NF145), partially denervated (<30% overlap) or fully denervated (0% overlap) (the number of samples is indicated in results). To determine the intraepidermal nerve fiber density (IENFD) in hind paw skin, ×20 magnification images were obtained using a Zeiss LSM800 confocal microscope (pinhole 12 µm). Two to three sections spanning different regions of the hind paw were analyzed per sample. The dermis-epidermis interface (*stratum basale*) was identified using DAPI staining and all PGP9.5-positive fibers crossing the interface were counted (free standing fiber fragments and branches were not considered as independent fibers). The linear skin length was measured at the upper layer of epidermis and the IENFD calculated by dividing the number of fibers by the linear skin length (expressed as fibers/mm). The experimenter was blinded to the samples' genotype during image analysis. Statistical analysis of NMJ innervation was performed using a chi-squared test for categorical variables and analysis of IENFD was calculated using an unpaired two-tailed *t*-test with Welch's correction. *p*-values are indicated in figures and statistical significance was recognized when *p* < .05.

## 2.8 | LCM and RNAseq of lumbar spinal cord motor neurons

Lumbar spinal cords of 1-year old mice were freshly dissected and immediately frozen in liquid nitrogen for the laser capture microdissection of motor neuron cell bodies. For LCM-seq and polyA-based-sequencing analyses all steps were carried out as previously described (Nichterwitz et al., 2016) with minor modifications. Briefly, spinal cord tissue was sectioned at 18 µm thickness onto PEN membrane glass slides (Zeiss) and a quick histological Nissl staining based on the Arcturus Histogene Staining Kit protocol was performed prior to capture. Pools of approximately 70 cells per sample were captured under a Leica DM6000R/CTR6500 microscope using the Leica LMD7000 system. Collected cells were lysed in 5 µl of 0.2% Triton-X100 (Sigma-Aldrich, in water) with 2 U/µl of RNase inhibitor (Takara) and 1 µM of DTT (Invitrogen). The library preparation protocol described in Nichterwitz et al. is based on the Smart-seq2 protocol (Picelli et al., 2013) and was used to directly prepare cDNA without prior RNA extraction. Sequencing libraries were prepared using a Nextera XT DNA library preparation Kit (Illumina). Five nanograms of cDNA from each sample were sequenced on a NovaSeq6000 (NovaSeq Control Software 1.6.0/RTA v3.4.4), using an S4-flowcell and generating paired reads of 151 bp in length. An average of 76.19 million reads were obtained per sample.

The sequencing reads were aligned to the mm10 mouse genome using STAR version 2.7.0e (Dobin et al., 2013) with parameter

“-outSAMstrandField” set to “intronMotif.” Aligned reads were assigned to genomic features with *rpkmforgenes.py* (Ramskold, Wang, Burge, & Sandberg, 2009) using Ensembl version GRCm38.95 as annotation. Parameters used in *rpkmforgenes.py* were “-fulltranscript” and “-rnameoverlap.” Differential expression was analyzed in R (version 3.4.4) with DESeq2 version 1.24.0 (Love, Huber, & Anders, 2014). Default settings were used and an FDR-adjusted *p*-value <.05 was considered significant. No genes were excluded a priori before the DESeq2 procedure.

### 3 | RESULTS

#### 3.1 | Generation of MCT1 and MCT4 SC-specific conditional knockout mouse models

In the CNS, expression of MCT1 by oligodendrocytes and MCT1/4 by astrocytes is necessary for the metabolic support of neurons. Namely, MCT1 depletion in oligodendrocytes leads to axonal damage and it is reduced in patients and animal models of amyotrophic lateral sclerosis

(Lee et al., 2012). Astrocytic MCT4, on the other hand, is essential for long-term memory formation (Suzuki et al., 2011) and its absence can be rescued by administration of lactate that can be directly taken up by neurons via MCT2. The presence of MCT1 and MCT4 in SCs (Domenech-Estevéz et al., 2015) prompted us to question if a similar role for MCTs could be observed in the PNS. We therefore established two conditional knockout mouse models in which exon 5 of MCT1 and exons 3–5 of MCT4 were eliminated from SC specifically using mice expressing Cre recombinase under the control of the myelin protein zero promoter (MPZ-Cre; Feltri et al., 1999) (Figure 1a). Depletion of either MCT1 or MCT4 was validated by qPCR in endoneurium of sciatic nerves isolated from 1-month old mice, without concomitant changes in the remaining MCTs (Figure 1b). To further demonstrate the effect of induced deletion on protein expression, we performed Western blotting of 1-month old MCT1 control and cKO sciatic nerves, which showed a >50% reduction in MCT1 levels (Figure 1c), and 11-day old MCT4 control and cKO sciatic nerves, showing a reduction of approximately 40% of MCT4 levels. (Figure 1d). The reduced level of mRNA and protein was further confirmed by qPCR and Western blotting of 1 year old MCT1 samples, as

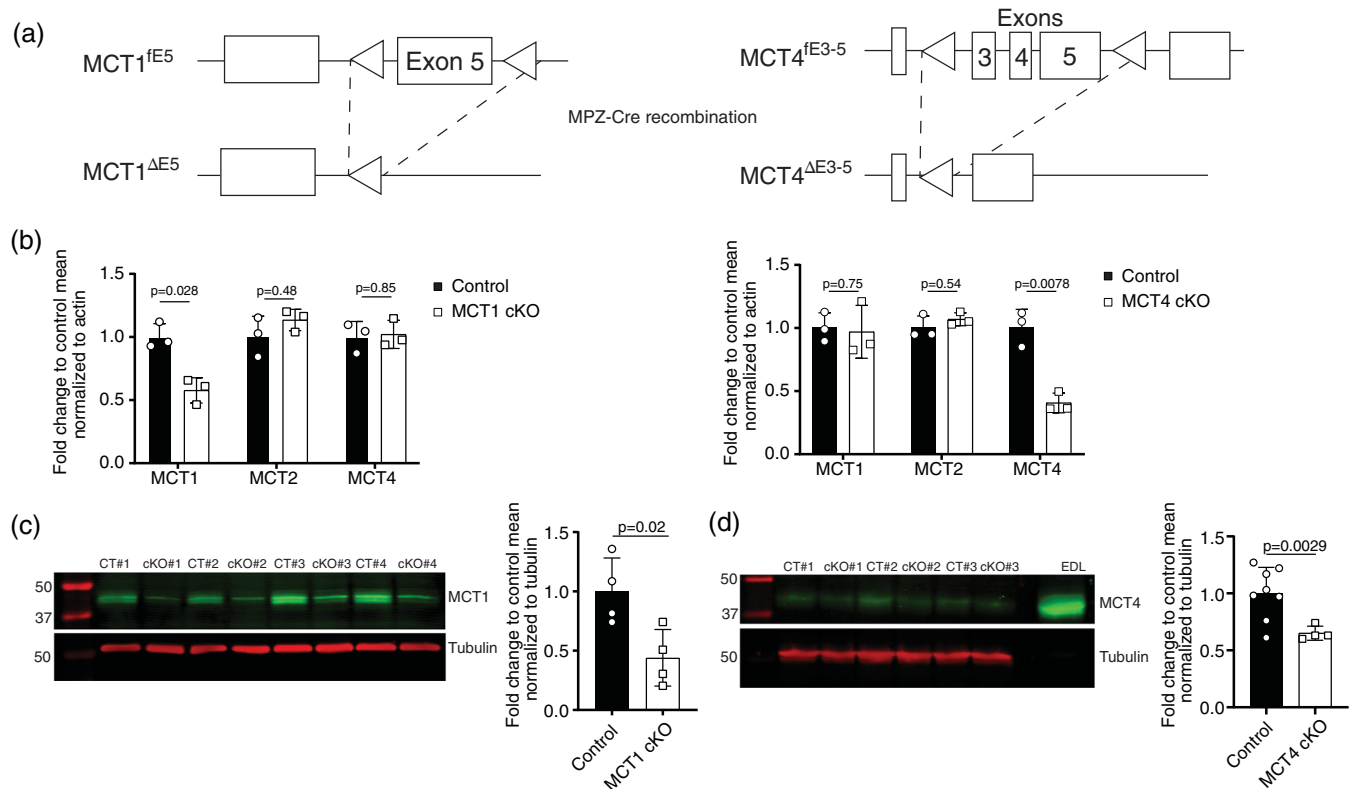


**FIGURE 1** Development of Schwann cell-specific MCT1 and MCT4 conditional knockout mice. (a) Schematic representation of MCT1 and MCT4 floxed alleles, and the result of MPZ-Cre-mediated recombination in SC. (b) Expression levels of MCT1, MCT2, and MCT4 in 1-month old sciatic nerves isolated from control and cKO mice, normalized to actin (data are expressed as mean  $\pm$  SD, two-tailed *t*-test with Welch's correction, number of samples [indicated by open circles and squares] and *p*-values are presented in the graphs). (c) Western blot and quantification of MCT1 in protein lysates from 1-month old sciatic nerves isolated from control and MCT1 cKO mice, tubulin was used as internal control (data are expressed as mean  $\pm$  SD, two-tailed *t*-test with Welch's correction, number of samples, and *p*-values are indicated in the graph). (d) Western blot and quantification of MCT4 in protein lysates from 11-days old sciatic nerves isolated from control and MCT4 cKO mice, tubulin was used as internal control, extensor digitorum longus (EDL) was used as positive control for MCT4 expression. (data are expressed as mean  $\pm$  SD, two-tailed *t*-test with Welch's correction, number of samples, and *p*-values are indicated in the graph) [Color figure can be viewed at [wileyonlinelibrary.com](http://wileyonlinelibrary.com)]

well as by immunohistochemistry on MCT4 teased sciatic nerve fibers (Supplemental Figure 1).

### 3.2 | MCT1 and MCT4 cKO mice do not present detectable alteration in their PNS function

Mutant mice developed overall normally, were fertile, and lived for as long as their wild-type littermates. To characterize the function of peripheral nerves, we performed nerve conduction velocity studies on both motor (MNCV) and sensory (SNCV) tracts in 1-year old animals. MNCV measurements were performed on the sciatic nerve while SNCV was measured on the tail. We did not detect any measurable difference between control and cKO animals in either MNCV or in SNCV (Figure 2a,b). To complement these observations, we performed one motor behavioral test—catwalk—and three sensory tests—von Frey filaments for mechanical sensitivity, Hargreaves box for heat and acetone test for cold sensation. The sensory tests showed that mechanical and thermal sensitivities are preserved in the absence of glial MCT1 or MCT4 except for a minor (1 s,  $p = .04$ ) difference in withdrawal latency detected on MCT1 cKO males (Figure 2c and Supplemental Figure 2). The catwalk also showed similar results for

regularity index, speed and cadence (Figure 2d and Supplemental Figure 2). Taken together these data suggest that deletion of MCT1 or MCT4 in SC does not significantly affect nerve conduction velocity or motor and sensory behavior in mice at 1-year of age.

### 3.3 | Glial MCT1 is required for long-term maintenance of motor end-plate integrity

To detect potential structural changes in the PNS, we analyzed semi-thin sections of sciatic nerves from MCT1 cKO or MCT4 cKO mice. Samples from young animals (P10 and 4 months) showed no observable differences in the structure of peripheral nerve tracts in the absence of MCT1 or MCT4 (data not shown) leading us to conclude that nerves develop normally and, thus, to focus on a more in-depth analysis of 1-year old animals. Also in the aged animals, myelin and axons were preserved in both lines with no detectable differences in  $g$ -ratio and distribution of axonal calibers (Figure 3). The number of sciatic nerve myelinated fibers and the  $g$ -ratio of spinal roots were also unchanged (Supplemental Figure 3). Electron microscopy analysis of Remak bundles also failed to reveal any differences between control and cKO mice. The area occupied by unmyelinated fibers in

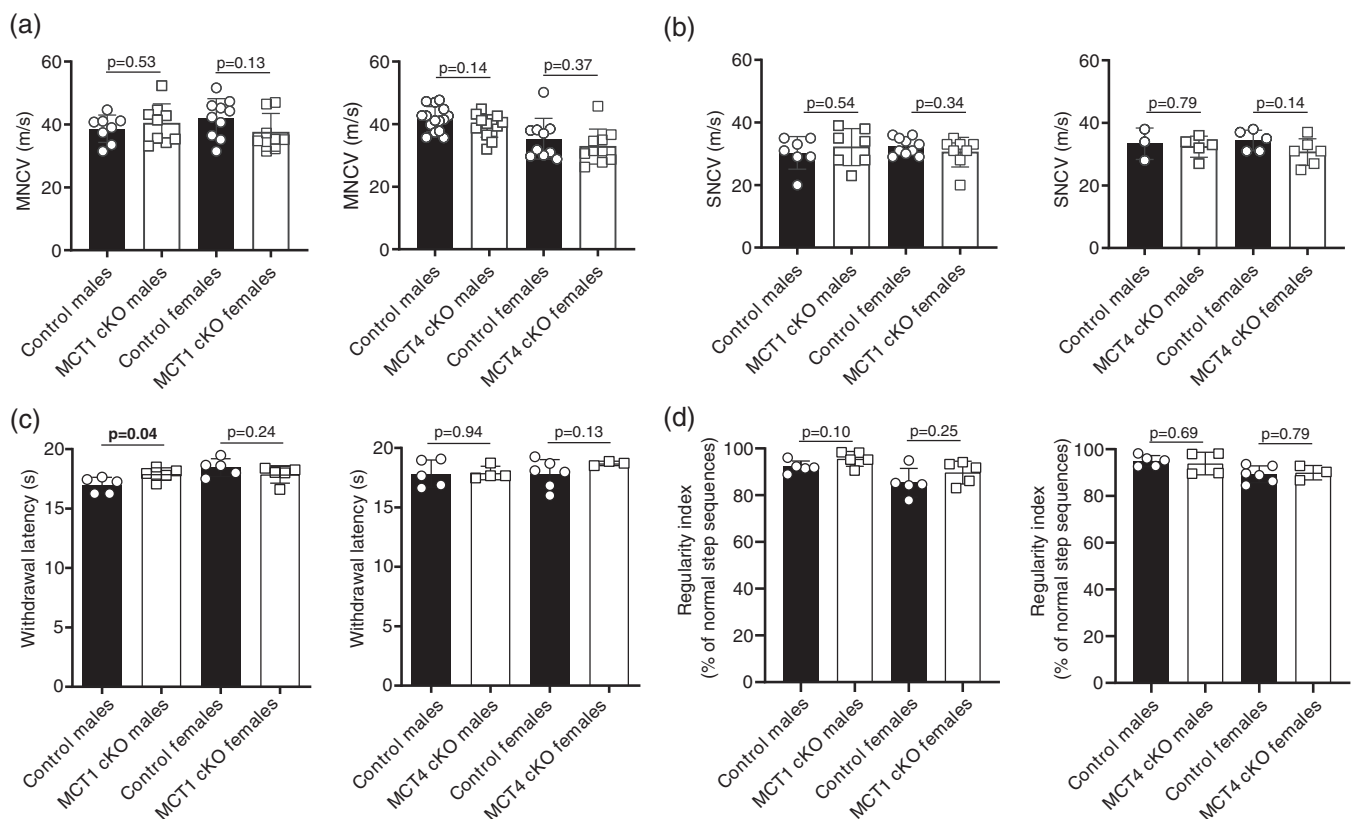


**FIGURE 2** Motor and sensory nerve functions are preserved in 1-year old MCT1 cKO and MCT4 cKO mice. (a) MNCV was determined in the hindlimbs and (b) SNCV in the tail of mice of both sexes. Data are expressed as mean  $\pm$  SD, two-tailed  $t$ -test with Welch's correction, number of animals (indicated by open circles and squares) and  $p$ -values are indicated in the graphs. (c) Results from the modified Hargreaves box test expressed as withdrawal latency in s, and (d) step regularity index obtained with the Catwalk test. Data are expressed as mean  $\pm$  SD, analysis by unpaired two-tailed  $t$ -test with Welch's correction, number of animals and  $p$ -values are indicated in the graphs

MCT1 cKO or MCT4 cKO was similar to control, as well as the distribution of number of axons per bundle and the presence of axons greater than 1  $\mu\text{m}$  in diameter (Figure 4).

We hypothesized that the impact of ablating MCT expression in SC could be affecting neurons in a subclinical manner that cannot be detected in the proximal/central part of the sciatic nerve or behavior

of cKO mice. We therefore analyzed the most distal part of sciatic nerve, concentrating on the innervation status of neuromuscular junctions (NMJ) in the gastrocnemius muscle and the density of free nerve endings in the hind paw skin of 1-year old mice. We focused on MCT1 cKO since MCT1 has higher level of expression in SC (Domenech-Estevéz et al., 2015; Halestrap, 2013). We found that the

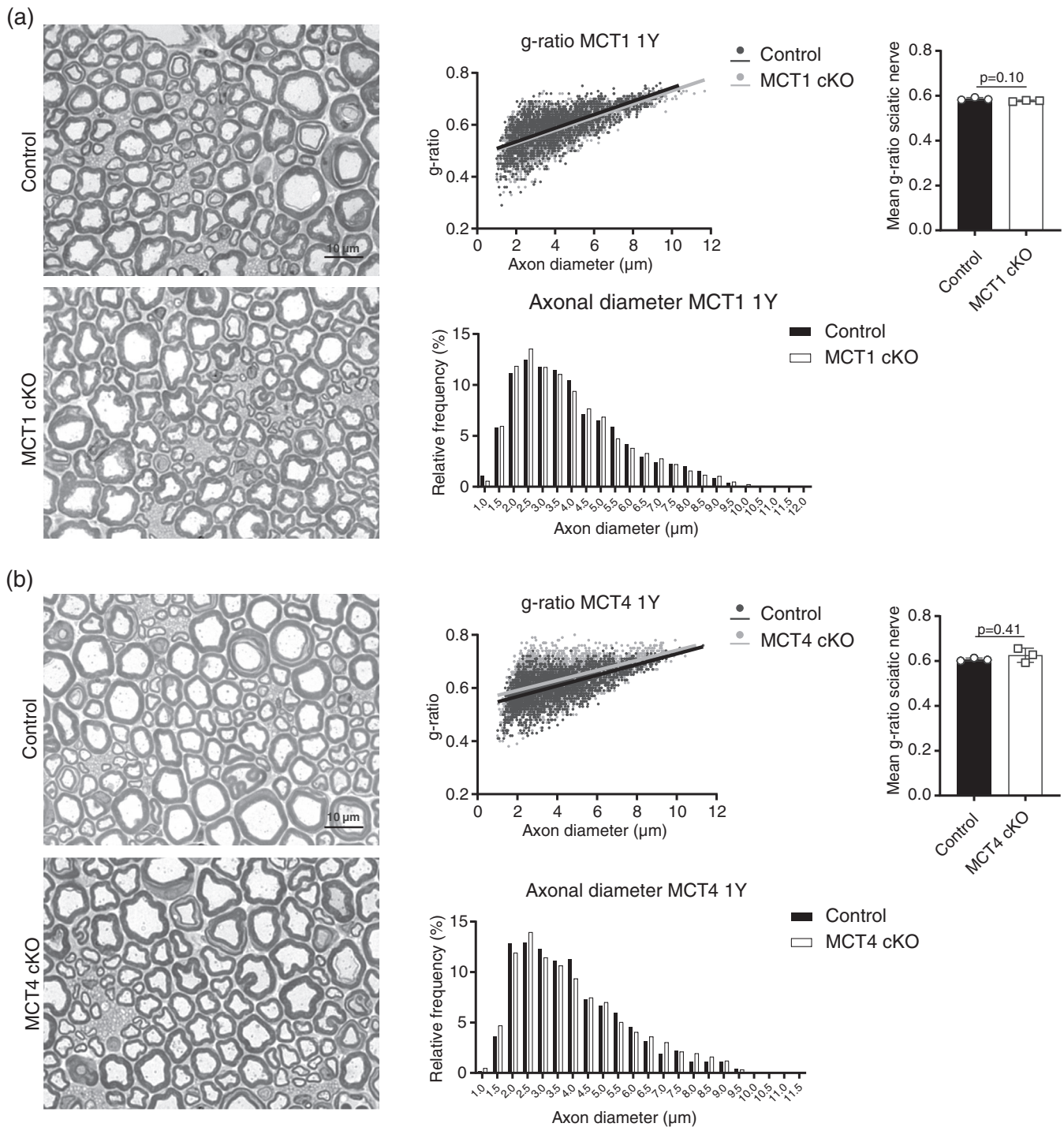


**FIGURE 3** Myelin thickness and axonal diameter are maintained in the absence of MCT1 or MCT4. Left panels: light microscopy images of 1-year old sciatic nerve semi-thin sections stained with toluidine blue (100 $\times$  magnification). Right panels: graphical representations of g-ratio, mean g-ratio and axonal diameter for MCT1 (a) and MCT4 (b) cKO mice. Mean g-ratio data are expressed as mean  $\pm$  SD, two-tailed *t*-test with Welch's correction, number of samples and *p*-values are indicated in the graphs



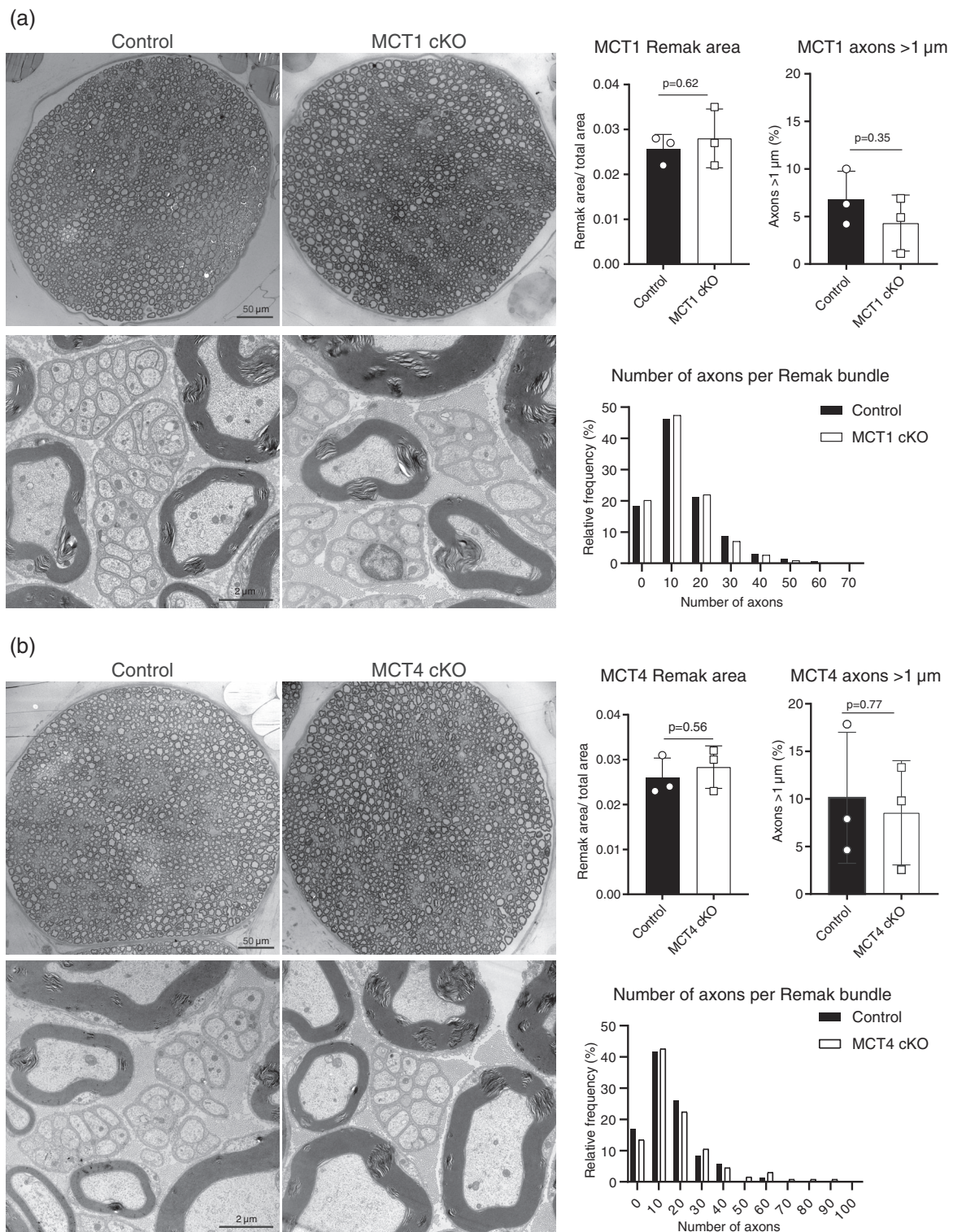


**FIGURE 4** Unmyelinated Remak bundles are preserved in the absence of MCT1 or MCT4. Left panels: transmission electron microscopy images of ultra-thin sections from 1-year old sciatic nerve (top—1,200 $\times$ , bottom—11,000 $\times$  magnification). Right panels: graphical representations of area occupied by Remak bundles, number of unsorted axons ( $>1 \mu\text{m}$ ) and number of axons per bundle for MCT1 (a) and MCT4 (b) cKO mice. Data are expressed as mean  $\pm$  SD, two-tailed *t*-test with Welch's correction, number of samples and *p*-values are indicated in the graphs

intraepidermal nerve fiber density (IENFD) was unchanged in MCT1 cKO as compared to control (Figure 5a). However, the percentage of fully innervated NMJ was reduced and accompanied by a concomitant increase in fully denervated and partially denervated NMJs, revealing

that MCT1 expressed by SC has a role in the maintenance of motor end-plate innervation (Figure 5b). This effect had a late onset, as changes in NMJ innervation were not detected at 6-months of age (Supplemental Figure 4).

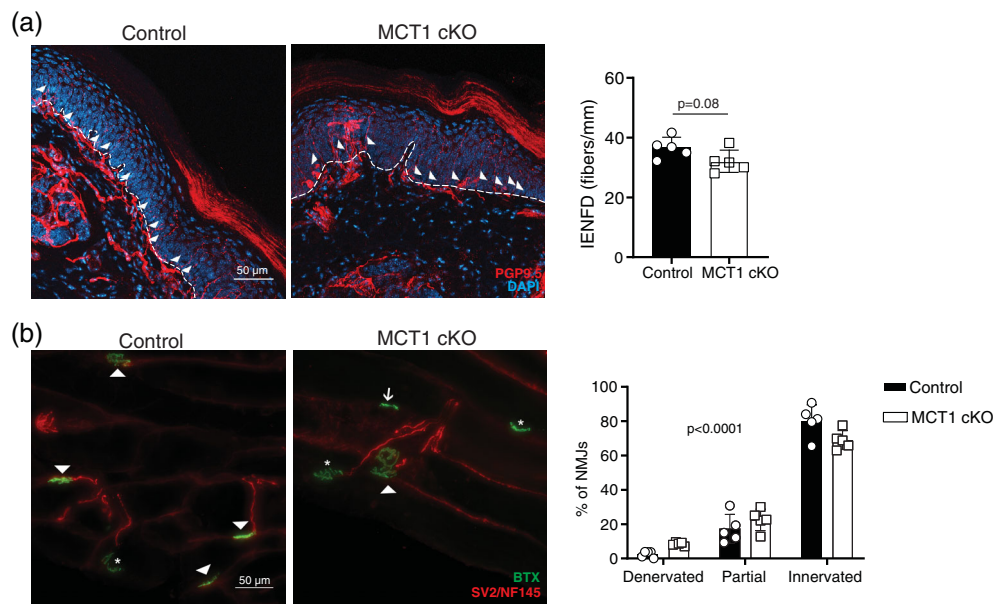


**FIGURE 5** Distal innervation of muscle, but not skin, is impaired in 1-year old MCT1 cKO mice. (a) Hind paw skin sections of 1-year old mice stained with DAPI (blue) and PGP9.5 (red) to visualize free nerve endings. Dashed line indicates dermis-epidermis interface and arrowheads indicate individual nerve endings projecting from the dermis into the epidermis. Graph represents the intraepidermal nerve fiber density (number of fibers divided by the linear length of skin). Data are expressed as mean  $\pm$  SD, unpaired two-tailed *t*-test with Welch's correction, number of samples and *p*-value are indicated in graph. (b) Sections of gastrocnemius muscle stained with fluorescently labeled bungarotoxin (green, indicates post-synaptic neuromuscular junction or NMJ) and SV2 + NF145 (red, indicates pre-synaptic terminals). Arrow—denervated NMJ, asterisk—partial denervation, arrowhead—fully innervated NMJ. Graph represents the percentage of NMJs in each category. Data are expressed as mean  $\pm$  SD,  $\chi^2$ -test for categorical variables was performed on the total number of observed NMJs, number of samples and *p*-value are indicated in graph [Color figure can be viewed at wileyonlinelibrary.com]

### 3.4 | Characterization of the transcriptional landscape in motor neurons of MCT1 cKO mice

The localized structural alterations detectable only in the distal part of the PNS in MCT1 cKO mice led us to suspect that there might be pre-symptomatic molecular changes in motor neurons that escaped our phenotypic characterization. To address this hypothesis, we performed laser capture microdissection of lumbar motor neuron cell bodies and sequenced their transcriptome using LCM-seq (Nichterwitz et al., 2016) (Figure 6a, Supplemental Figure 5). To control the specificity of the captured neuronal population, we first interrogated the level of expression of genes known to be specific for motor neurons or other neuronal populations. As expected, we observed high levels of *Chat*, *Isl1/2*, and *Mnx1(Hb9)* which are known to be present in motor neurons (Stifani, 2014) while the expression of *Gata2/3*, *Sox14*, and *Chx10*, expressed by interneurons (Gosgnach et al., 2017; Lu, Niu, & Alaynick, 2015), was absent (Supplemental file 2). Comparison of control and cKO motor neuron transcriptomes revealed 121 differentially expressed transcripts of which 73 had a known function, with 39 upregulated genes in the cKO and 34 downregulated (Figure 6b, Supplemental file 2). The small number of genes identified made gene ontology enrichment analysis (GO analysis, <http://geneontology.org/>) statistically insignificant, so we manually categorized them based on GO Biological Function (<https://www.ebi.ac.uk/QuickGO/>) (Figure 6b).

We found genes related to immune response, classical signaling pathways (MAPK, GPCR), protein synthesis and degradation and autophagy to be affected in both groups. A small number of genes related to cell adhesion and glycosylation were exclusively upregulated while genes involved in NF $\kappa$ B signaling and a voltage-gated potassium channel were downregulated. Notably, many zinc-finger proteins with predicted transcription-repressing motives were upregulated together with genes involved in lipid metabolism, mitochondria, and oxidative stress. Consistent with the observed neuromuscular denervation, several cytoskeletal genes were downregulated (Figure 6c). These results suggest that the absence of MCT1 in SC, and consequently a reduced ability to support axonal metabolism, is inducing a transcriptional shift in motor neurons potentially aiming to compensate energetic needs and sustain neuronal survival.

## 4 | DISCUSSION

In this work, we described two conditional knockout models in which MCT1 or MCT4 were eliminated specifically in SCs. We found that absence of MCTs from SC does not affect the development of the PNS, as these mice present normal myelin, nerve conduction velocities and motor and sensory behavior. Interestingly, we discovered that MCT1 (but not MCT4) expression in SC is necessary for long-term

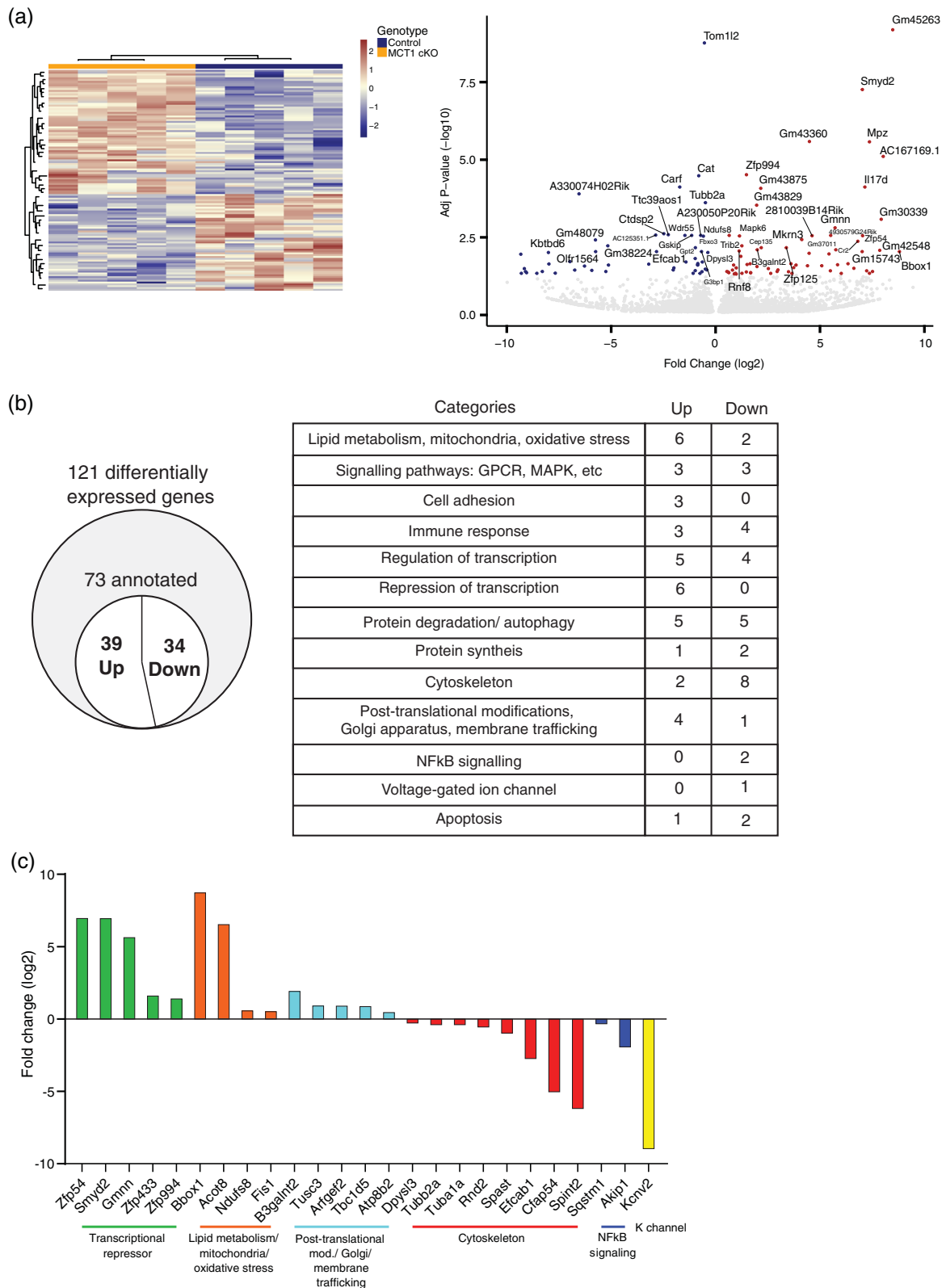


**FIGURE 6** Absence of MCT1 in Schwann cells induces changes in gene expression in lumbar motor neurons. (a) Heatmap and volcano plot of differentially expressed transcripts between LCM-dissected motor neurons from control and MCT1 cKO mice. (b) Number of differentially expressed genes in lumbar motor neurons of 1-year old MCT1 cKO mice. Gene function categories identified based on GO Biological Function and number of genes upregulated and downregulated for each category. (c) Examples of gene expression fold changes from selected functional categories [Color figure can be viewed at [wileyonlinelibrary.com](http://wileyonlinelibrary.com)]



maintenance of neuromuscular junction innervation and is associated with transcriptional changes in lumbar motor neurons, suggesting that SC metabolic support to axons is necessary for proper maintenance of motor neuron function. These neurons seem to compensate for the absence of SC-mediated support by upregulating genes involved in mitochondrial function, regulation of transcription and glycosylation, which is important for the function of many transmembrane proteins such as receptors of neurotransmitters and for cell adhesion. Of particular interest, *Erk3*, *Ndufs8*, and *Fis1* were found to be upregulated, while *Tuba1a*, *Rnd2*, *G3bp1*, and *Akip1* were downregulated. *Erk3*, also known as *Mapk6*, is an atypical mitogen-activated protein kinase (MAPK) and is involved in dendritic spine formation and development of the nervous system (Brand et al., 2012); *Ndufs8* is an essential subunit of mitochondrial NADH:ubiquinone oxidoreductase, or complex I (Procaccio et al., 1997), and its presence is necessary for oxidative phosphorylation, and *Fis1* is a positive regulator of mitochondrial fission (Loson, Song, Chen, & Chan, 2013). *Tuba1a* ( $\alpha$ -Tubulin 1A) is a component of the neuronal cytoskeleton (Pubmed gene ID 22142) (Yue et al., 2014) and *Rnd2* is a member of the Rho GTPase family involved in regulation of actin cytoskeleton, and is involved in dendrite branching (Negishi & Katoh, 2005). *Akip1* promotes the phosphorylation of NFkB subunit p65/RelA by PKA, increasing its retention in the nucleus and enhancing expression of NFkB target genes (Gao, Asamitsu, Hibi, Ueno, & Okamoto, 2008), and conditional knockout of RelA in neurons promotes their regeneration (Haenold et al., 2014), while G3BP1 regulates the formation of stress granules and prevents axonal regeneration (Sahoo et al., 2018). The upregulation of mitochondria-related genes could be a response to reduced metabolic support from SC. The downregulated cytoskeletal genes support the observation of denervation while downregulation of *Akip1*, a regulator of NFkB signaling via RelA, and G3BP1, an inhibitor of axon regeneration, could be an attempt at preservation of axons (Haenold et al., 2014; Sahoo et al., 2018). The mild effect observed is not surprising, given the fact that non-demyelinating peripheral neuropathies can often start in the later decades of life in humans, progress in a distal-to-proximal fashion and present widely ranging symptoms, from mild foot deformities and difficulty in running, to needing walking aids and an inability to evoke motor potentials in lower limbs (Senderek et al., 2000). It is possible that the time point analyzed in this work, which corresponds to human middle age (approximately 40 years old) (Flurkey, Curren, & Harrison, 2007), reflects the onset of the phenotype which may worsen with aging.

Recent work by Jha and colleagues (Jha et al., 2019) described a SC-specific MCT1 conditional knockout (generated by deletion of exon 2) with a predominantly sensory phenotype. These mice presented progressive thinning of myelin in the sural nerve and increased nodal length, which correlated with reduced SNCV and mechanical sensitivity. This was linked to altered lipid metabolism, reduced expression of MAG and increased expression of c-Jun, suggesting that MCT1 cKO SC may be regressing to less mature states. The authors suggested that ablation of MCT1 from SC was not sufficient to affect glial support to axons. Our observations revealed transcriptional and localized structural changes in the terminals of axons that are in

contact with MCT1-deficient SCs which were not characterized in the other model (Jha et al., 2019). It is also possible that the differences observed between these two studies could be due to the different genetic backgrounds of the models. Considering the relatively mild phenotype we observed, we hypothesize, as Jha et al. also defended, that the remaining MCTs expressed by SC can compensate partially for the MCT1 deficiency. This hypothesis should be further evaluated by generation and characterization of a model missing multiple or all MCTs in SC.

The past decade has been rich in discoveries related to metabolic interactions between glia and neurons. In mammalian systems, the astrocyte-to-neuron lactate shuttle (Pellerin et al., 2007) is essential for long-term memory formation (Suzuki et al., 2011) and oligodendrocytes stimulated with NMDA receptor agonists are able to sustain axonal activity *ex vivo*, linking neuronal activity with glial support (Saab et al., 2016). In the PNS, the knockout of major metabolic regulator LKB1 in SC was shown to lead to axonal degeneration without myelin loss and was accompanied by a neuroprotective increase in lactate release (Beirowski et al., 2014). Our present data show that MCTs expressed by peripheral myelinating glia, which are able to transport lactate, are important for long-term maintenance of motor end-plate innervation, independently of myelin itself. Terminal SC (Griffin & Thompson, 2008) could also play a role in this process; however, the previously published data indicate that terminal SC at neuromuscular junctions do not express MCT1 (Morrison et al., 2015). To further our understanding of SC–neuron metabolic interactions, it would be relevant to study the absence of multiple MCTs in SC and/or the absence of neuronal MCTs. These studies could have implications for the comprehension and treatment of amyotrophic lateral sclerosis and peripheral neuropathies such as axonal forms of Charcot–Marie–Tooth disease and diabetic neuropathy.

#### ACKNOWLEDGMENTS

We would like to thank Hasna Baloui and Enric Domènech-Estévez for their help with preliminary sample collection and analysis of sciatic nerves from MCT1 and 4 cKO and Ana Carolina Temporão for her help with sample preparation and immunohistochemistry. We would also like to thank Klaus Nave for providing us with the MCT1 antibody and Jean-Michel Vallat for advice concerning electron microscopy. The RNA-seq mapping computations were performed on resources provided by SNIC through the Uppsala Multidisciplinary Center for Advanced Computational Science (UPPMAX) under project SNIC 2018/8-327. This work was supported by Swedish StratNeuro program grant (to R. C.), Swedish Research Council grant 2015-02394 (to R. C.), 2016-02112 (to E. H.), (2013-8373) to C. I. S., Knut och Alice Wallenbergs Stiftelse grant (to C. I. S.) and KID program grants (to R. C. and C. I. S.). L. P. received financial support for this project from the Department of Physiology, University of Lausanne, Switzerland and from the program IdEx Bordeaux ANR-10-IDEX-03-02.

#### DATA AVAILABILITY STATEMENT

The data that support the findings of this study are available from the corresponding author upon reasonable request.

## ORCID

Roman Chrast  <https://orcid.org/0000-0003-4189-3514>

## REFERENCES

- Angeby Moller, K., Svard, H., Suominen, A., Immonen, J., Holappa, J., & Stenfors, C. (2018). Gait analysis and weight bearing in pre-clinical joint pain research. *Journal of Neuroscience Methods*, 300, 92–102. <https://doi.org/10.1016/j.jneumeth.2017.04.011>
- Arnaud, E., Zenker, J., de Preux Charles, A. S., Stendel, C., Roos, A., Medard, J. J., ... Chrast, R. (2009). SH3TC2/KIAA1985 protein is required for proper myelination and the integrity of the node of Ranvier in the peripheral nervous system. *Proceedings of the National Academy of Sciences of the United States of America*, 106(41), 17528–17533. <https://doi.org/10.1073/pnas.0905523106>
- Bartesaghi, L., Arnaud Gouttenoire, E., Prunotto, A., Médard, J. J., Bergmann, S., & Chrast, R. (2015). Sox4 participates in the modulation of Schwann cell myelination. *The European Journal of Neuroscience*, 42(2), 1788–1796. <https://doi.org/10.1111/ejn.12929>
- Beirowski, B., Babetto, E., Golden, J. P., Chen, Y. J., Yang, K., Gross, R. W., ... Milbrandt, J. (2014). Metabolic regulator LKB1 is crucial for Schwann cell-mediated axon maintenance. *Nature Neuroscience*, 17(10), 1351–1361. <https://doi.org/10.1038/nn.3809>
- Brady, S. T., & Lasek, R. J. (1981). Nerve-specific enolase and creatine phosphokinase in axonal transport: Soluble proteins and the axoplasmic matrix. *Cell*, 23(2), 515–523. [https://doi.org/10.1016/0092-8674\(81\)90147-1](https://doi.org/10.1016/0092-8674(81)90147-1)
- Brand, F., Schumacher, S., Kant, S., Menon, M. B., Simon, R., Turgeon, B., ... Kotlyarov, A. (2012). The extracellular signal-regulated kinase 3 (mitogen-activated protein kinase 6 [MAPK6])-MAPK-activated protein kinase 5 signaling complex regulates septin function and dendrite morphology. *Molecular and Cellular Biology*, 32(13), 2467–2478. <https://doi.org/10.1128/MCB.06633-11>
- Chaplan, S. R., Bach, F. W., Pogrel, J. W., Chung, J. M., & Yaksh, T. L. (1994). Quantitative assessment of tactile allodynia in the rat paw. *Journal of Neuroscience Methods*, 53(1), 55–63. [https://doi.org/10.1016/0165-0270\(94\)90144-9](https://doi.org/10.1016/0165-0270(94)90144-9)
- Dirig, D. M., Salami, A., Rathbun, M. L., Ozaki, G. T., & Yaksh, T. L. (1997). Characterization of variables defining hindpaw withdrawal latency evoked by radiant thermal stimuli. *Journal of Neuroscience Methods*, 76(2), 183–191. [https://doi.org/10.1016/s0165-0270\(97\)00097-6](https://doi.org/10.1016/s0165-0270(97)00097-6)
- Dixon, W. J. (1980). Efficient analysis of experimental observations. *Annual Review of Pharmacology and Toxicology*, 20, 441–462. <https://doi.org/10.1146/annurev.pa.20.040180.002301>
- Dobin, A., Davis, C. A., Schlesinger, F., Drenkow, J., Zaleski, C., Jha, S., ... Gingeras, T. R. (2013). STAR: ultrafast universal RNA-seq aligner. *Bioinformatics*, 29(1), 15–21. <https://doi.org/10.1093/bioinformatics/bts635>
- Domenech-Estevéz, E., Baloui, H., Repond, C., Rosafio, K., Medard, J. J., Tricaud, N., ... Chrast, R. (2015). Distribution of monocarboxylate transporters in the peripheral nervous system suggests putative roles in lactate shuttling and myelination. *The Journal of Neuroscience*, 35(10), 4151–4156. <https://doi.org/10.1523/JNEUROSCI.3534-14.2015>
- Feltri, M. L., D'Antonio, M., Previtali, S., Fasolini, M., Messing, A., & Wrabetz, L. (1999). P0-Cre transgenic mice for inactivation of adhesion molecules in Schwann cells. *Annals of the New York Academy of Sciences*, 883, 116–123 Retrieved from <https://www.ncbi.nlm.nih.gov/pubmed/10586237>
- Flurkey, K., Curren, J., & Harrison, D. (2007). The mouse in aging research. In J. G. Fox (Ed.), *The mouse in biomedical research* (2nd ed., pp. 637–672). Burlington, MA: American College Laboratory Animal Medicine (Elsevier).
- Gao, N., Asamitsu, K., Hibi, Y., Ueno, T., & Okamoto, T. (2008). AKIP1 enhances NF-kappaB-dependent gene expression by promoting the nuclear retention and phosphorylation of p65. *The Journal of Biological Chemistry*, 283(12), 7834–7843. <https://doi.org/10.1074/jbc.M710285200>
- Gosgnach, S., Bikoff, J. B., Dougherty, K. J., El Manira, A., Lanuza, G. M., & Zhang, Y. (2017). Delineating the diversity of spinal interneurons in locomotor circuits. *The Journal of Neuroscience*, 37(45), 10835–10841. <https://doi.org/10.1523/jneurosci.1829-17.2017>
- Griffin, J. W., & Thompson, W. J. (2008). Biology and pathology of non-myelinating Schwann cells. *Glia*, 56(14), 1518–1531. <https://doi.org/10.1002/glia.20778>
- Haenold, R., Weih, F., Herrmann, K. H., Schmidt, K. F., Krempler, K., Engelmann, C., ... Kretz, A. (2014). NF-kappaB controls axonal regeneration and degeneration through cell-specific balance of RelA and p50 in the adult CNS. *Journal of Cell Science*, 127(Pt 14), 3052–3065. <https://doi.org/10.1242/jcs.140731>
- Halestrap, A. P. (2013). Monocarboxylic acid transport. *Comprehensive Physiology*, 3(4), 1611–1643. <https://doi.org/10.1002/cphy.c130008>
- Hirrlinger, J., & Nave, K. A. (2014). Adapting brain metabolism to myelination and long-range signal transduction. *Glia*, 62(11), 1749–1761. <https://doi.org/10.1002/glia.22737>
- Jha, M. K., Lee, Y., Russell, K. A., Yang, F., Dastgheyb, R. M., Deme, P., ... Morrison, B. M. (2019). Monocarboxylate transporter 1 in Schwann cells contributes to maintenance of sensory nerve myelination during aging. *Glia*, 68, 161–177. <https://doi.org/10.1002/glia.23710>
- Lee, Y., Morrison, B. M., Li, Y., Lengacher, S., Farah, M. H., Hoffman, P. N., ... Rothstein, J. D. (2012). Oligodendroglia metabolically support axons and contribute to neurodegeneration. *Nature*, 487(7408), 443–448. <https://doi.org/10.1038/nature11314>
- Loson, O. C., Song, Z., Chen, H., & Chan, D. C. (2013). Fis1, Mff, MiD49, and MiD51 mediate Drp1 recruitment in mitochondrial fission. *Molecular Biology of the Cell*, 24(5), 659–667. <https://doi.org/10.1091/mbc.E12-10-0721>
- Love, M. I., Huber, W., & Anders, S. (2014). Moderated estimation of fold change and dispersion for RNA-seq data with DESeq2. *Genome Biology*, 15(12), 550. <https://doi.org/10.1186/s13059-014-0550-8>
- Lu, D. C., Niu, T., & Alaynick, W. A. (2015). Molecular and cellular development of spinal cord locomotor circuitry. *Frontiers in Molecular Neuroscience*, 8, 25. <https://doi.org/10.3389/fnmol.2015.00025>
- Machler, P., Wyss, M. T., Elsayed, M., Stobart, J., Gutierrez, R., von Faber-Castell, A., ... Weber, B. (2016). In vivo evidence for a lactate gradient from astrocytes to neurons. *Cell Metabolism*, 23(1), 94–102. <https://doi.org/10.1016/j.cmet.2015.10.010>
- Meyer, N., Richter, N., Fan, Z., Siemonsmeier, G., Pivneva, T., Jordan, P., ... Kettenmann, H. (2018). Oligodendrocytes in the mouse corpus callosum maintain axonal function by delivery of glucose. *Cell Reports*, 22(9), 2383–2394. <https://doi.org/10.1016/j.celrep.2018.02.022>
- Morrison, B. M., Tsingalia, A., Vidensky, S., Lee, Y., Jin, L., Farah, M. H., ... Rothstein, J. D. (2015). Deficiency in monocarboxylate transporter 1 (MCT1) in mice delays regeneration of peripheral nerves following sciatic nerve crush. *Experimental Neurology*, 263, 325–338. <https://doi.org/10.1016/j.expneurol.2014.10.018>
- Nave, K. A. (2010). Myelination and the trophic support of long axons. *Nature Reviews Neuroscience*, 11(4), 275–283. <https://doi.org/10.1038/nrn2797>
- Negishi, M., & Katoh, H. (2005). Rho family GTPases and dendrite plasticity. *The Neuroscientist*, 11(3), 187–191. <https://doi.org/10.1177/1073858404268768>
- Nichterwitz, S., Chen, G., Aguila Benitez, J., Yilmaz, M., Storz, H., Cao, M., ... Hedlund, E. (2016). Laser capture microscopy coupled with smart-seq2 for precise spatial transcriptomic profiling. *Nature Communications*, 7, 12139. <https://doi.org/10.1038/ncomms12139>
- Pellerin, L., Bouzier-Sore, A. K., Aubert, A., Serres, S., Merle, M., Costalat, R., & Magistretti, P. J. (2007). Activity-dependent regulation of energy metabolism by astrocytes: An update. *Glia*, 55(12), 1251–1262. <https://doi.org/10.1002/glia.20528>



- Picelli, S., Bjorklund, A. K., Faridani, O. R., Sagasser, S., Winberg, G., & Sandberg, R. (2013). Smart-seq2 for sensitive full-length transcriptome profiling in single cells. *Nature Methods*, 10(11), 1096–1098. <https://doi.org/10.1038/nmeth.2639>
- Pierre, K., Magistretti, P. J., & Pellerin, L. (2002). MCT2 is a major neuronal monocarboxylate transporter in the adult mouse brain. *Journal of Cerebral Blood Flow & Metabolism*, 22(5), 586–595. <https://doi.org/10.1097/00004647-200205000-00010>
- Procaccio, V., Depetris, D., Soularue, P., Mattei, M. G., Lunardi, J., & Issartel, J. P. (1997). cDNA sequence and chromosomal localization of the NDUFS8 human gene coding for the 23 kDa subunit of the mitochondrial complex I. *Biochimica et Biophysica Acta*, 1351(1–2), 37–41. [https://doi.org/10.1016/s0167-4781\(97\)00020-1](https://doi.org/10.1016/s0167-4781(97)00020-1)
- Ramskold, D., Wang, E. T., Burge, C. B., & Sandberg, R. (2009). An abundance of ubiquitously expressed genes revealed by tissue transcriptome sequence data. *PLoS Computational Biology*, 5(12), e1000598. <https://doi.org/10.1371/journal.pcbi.1000598>
- Saab, A. S., Tzvetavona, I. D., Trevisiol, A., Baltan, S., Dibaj, P., Kusch, K., ... Nave, K. A. (2016). Oligodendroglial NMDA receptors regulate glucose import and axonal energy metabolism. *Neuron*, 91(1), 119–132. <https://doi.org/10.1016/j.neuron.2016.05.016>
- Sahoo, P. K., Lee, S. J., Jaiswal, P. B., Alber, S., Kar, A. N., Miller-Randolph, S., ... Twiss, J. L. (2018). Axonal G3BP1 stress granule protein limits axonal mRNA translation and nerve regeneration. *Nature Communications*, 9(1), 3358. <https://doi.org/10.1038/s41467-018-05647-x>
- Schindelin, J., Arganda-Carreras, I., Frise, E., Kaynig, V., Longair, M., Pietzsch, T., ... Cardona, A. (2012). Fiji: An open-source platform for biological-image analysis. *Nature Methods*, 9(7), 676–682. <https://doi.org/10.1038/nmeth.2019>
- Senderek, J., Hermanns, B., Lehmann, U., Bergmann, C., Marx, G., Kabus, C., ... Schröder, J. M. (2000). Charcot-Marie-Tooth neuropathy type 2 and P0 point mutations: Two novel amino acid substitutions (Asp61Gly; Tyr119Cys) and a possible “hotspot” on Thr124Met. *Brain Pathology*, 10(2), 235–248. <https://doi.org/10.1111/j.1750-3639.2000.tb00257.x>
- Stifani, N. (2014). Motor neurons and the generation of spinal motor neurons diversity. *Frontiers in Cellular Neuroscience*, 8, 293. <https://doi.org/10.3389/fncel.2014.00293>
- Stumpf, S. K., Berghoff, S. A., Trevisiol, A., Spieth, L., Duking, T., Schneider, L. V., ... Saher, G. (2019). Ketogenic diet ameliorates axonal defects and promotes myelination in Pelizaeus-Merzbacher disease. *Acta Neuropathologica*, 138(1), 147–161. <https://doi.org/10.1007/s00401-019-01985-2>
- Suzuki, A., Stern, S. A., Bozdagi, O., Huntley, G. W., Walker, R. H., Magistretti, P. J., & Alberini, C. M. (2011). Astrocyte–neuron lactate transport is required for long-term memory formation. *Cell*, 144(5), 810–823. <https://doi.org/10.1016/j.cell.2011.02.018>
- Yue, F., Cheng, Y., Breschi, A., Vierstra, J., Wu, W., Ryba, T., ... Mouse, E. C. (2014). A comparative encyclopedia of DNA elements in the mouse genome. *Nature*, 515(7527), 355–364. <https://doi.org/10.1038/nature13992>

## SUPPORTING INFORMATION

Additional supporting information may be found online in the Supporting Information section at the end of this article.

**How to cite this article:** Bouçanova F, Pollmeier G, Sandor K, et al. Disrupted function of lactate transporter MCT1, but not MCT4, in Schwann cells affects the maintenance of motor end-plate innervation. *Glia*. 2021;69:124–136. <https://doi.org/10.1002/glia.23889>